# A Clinical Prototype for Active Microwave Imaging of the Breast

Paul M. Meaney, *Member, IEEE*, Margaret W. Fanning, Dun Li, Steven P. Poplack, and Keith D. Paulsen, *Member, IEEE*

***Abstract*—Despite its recognized value in detecting and characterizing breast disease, X-ray mammography has important limitations that motivate the quest for alternatives to augment the diagnostic tools that are currently available to the radiologist. The rationale for pursuing electromagnetic methods is strong given: the data in the literature, which show that the electromagnetic properties of breast malignancy are significantly different than normal in the high megahertz to low gigahertz spectral range, microwave illumination can effectively penetrate the breast at these frequencies, and the breast is a small readily accessible tissue volume, making it an ideal site for deploying advanced near-field imaging concepts that exploit model-based image reconstruction methodology. In this paper, a clinical prototype of a microwave imaging system, which actively illuminates the breast with a 16-element transceiving monopole antenna array in the 300–1000-MHz range, is reported. Microwave exams have been delivered to five women through a water-coupled interface to the pendant breast with the participant positioned prone on an examination table. This configuration has been found to be a practical, comfortable approach to microwave breast imaging. Sessions lasted 10–15 min per breast and included full tomographic data acquisition at seven different array heights beginning at the chest wall and moving anteriorly toward the nipple for seven different frequencies at each array position. This clinical experience appears to be the first report of active near-field microwave imaging of the breast and is certainly the first attempt to exploit model-based image reconstructions from *in vivo* breast data in order to convert the measured microwave signals into spatial maps of electrical permittivity and conductivity. While clearly preliminary, the results are encouraging and have supplied some interesting findings. Specifically, it appears that the average relative permittivity of the breast as a whole correlates with radiologic breast density categorization and may be considerably higher than previously published values, which have been based on *ex vivo* tissue specimens.**

## I. Introduction

In the U.S., breast cancer is the most common nonskin malignancy in women and the second leading cause of female cancer mortality. Approximately 180 000 new cases of breast cancer were diagnosed and approximately 44 000 deaths occurred in 1994 alone [1]. Breast cancer will occur in approximately one in eight women by the age of 90 years old. Detection of breast cancer at an early stage increases the likelihood of successful treatment and long-term survival. Screen film mammography is currently the most effective method of detecting asymptomatic breast cancer [2].

Despite its recognized value in detecting and characterizing breast disease, X-ray mammography has important limitations. Perhaps most significantly, screening mammography suffers from a high false-positive rate [3]. The abnormal or "call back" rate of standard screening mammography in community practice is approximately 11% [2], [4]. This results in a positive predictive value (PPV) for the standard screening examination of approximately 4% and a biopsy yield of 17%–21% [2], [4]. The false negative rate of mammography is also not insignificant and ranges from 4% to 34% [5] depending on the definition of a false negative and the length of follow-up after a "normal" mammogram. Screening mammography is less sensitive in women with radiographically dense breast tissue [6]–[8]. This is of particular concern because the amount of fibroglandular tissue may represent an independent risk factor for developing breast cancer [9], [10] and there is a significant proportion of "dense" breasts in younger women and older women receiving exogenous estrogen [7], [11]–[14]. Mammography has other drawbacks, including examinee tolerance of compression, variability in radiological interpretation, and radiation dose considerations. High-quality film-screen mammography depends on optimal breast compression to reduce image blurring due to motion and X-ray scatter. Unfortunately, compression is uncomfortable and may lead to lack of compliance with screening regimens. In addition, striking variation in mammography interpretation has been reported [15], [16]. The amount of radiation exposure is very low and is under stringent federal regulation [The Mammography Quality Standards Act of 1992 (MQSA)]. Nevertheless, there remains a hypothetical risk of inducing breast carcinoma of approximately 1/1 000 000 with the low levels of radiation currently employed [17].

As a result, there is considerable motivation for developing alternative and/or complementary imaging modalities for detecting and characterizing breast disease. Of the available options, electromagnetic sensing has generated significant interest and an array of techniques covering a broad spectrum of possibilities ranging from near-dc electric currents to optical wavelengths in the near infrared have been investigated [18]–[28]. Several of these technologies have progressed to the point where a sizable positive clinical experience has emerged [18], [21], [22]. Others have historically shown rather poor performance [24], [26], [28], although more recent evidence seems to sug-

Manuscript received February 26, 2000; revised April 26, 2000. This work was supported in part by the National Institutes of Health under Grant P01-CA80139-01 awarded by the National Cancer Institute.

P. M. Meaney, M. W. Fanning, and D. Li are with the Thayer School of Engineering, Dartmouth College, Hanover, NH 03755 USA.

S. P. Poplack is with the Department of Diagnostic Radiology, Dartmouth–Hitchcock Medical Center, Lebanon, NH 03756 USA and also with the Norris Cotton Cancer Center, Lebanon, NH 03756 USA.

K. D. Paulsen is with the Thayer School of Engineering, Dartmouth College, Hanover, NH 03755 USA and also with the Norris Cotton Cancer Center, Lebanon, NH 03756 USA.

Publisher Item Identifier S 0018-9480(00)09535-1.

gest that earlier studies were flawed by premature technology coupled to unrealistic expectations regarding the realization of a single new screening tool [22]. Active microwave-imaging methods spanning the high-megahertz to low-gigahertz regime would appear to offer excellent opportunities to supplement the arsenal of breast screening and/or characterization tools available to the radiologist despite the fact that microwave imaging has yet to reach any demonstrated level of clinical feasibility.

The rationale for pursuing active microwave illumination of the breast is strong. First and foremost, there is data in the literature [29], [30] that shows that the electrical property values (permittivity and conductivity) of normal and malignant human breast tissues differ by fivefold to tenfold over the microwave frequency range (up to 3 GHz). In fact, for normal and malignant human tissues of the same histological type, the largest difference in electrical properties has been observed in the mammary gland relative to colon, kidney, liver, lung, and muscle [29]. Others have shown a positive correlation between dielectric properties and the degree of subcutaneous fibrosis hypothesizing that localized vascular failure results in changes in the free and bound water compartments of breast tissue, which are reflected in the observed dielectric property changes [31]. Second, assuming a largely fatty composition, the breast is relatively penetrable with microwaves that extends the usable frequency range to several gigahertz without placing unrealistic demands on the dynamic range that would be needed in a hardware system. Even if the breast as a whole is more lossy than the low-end estimates provided by *ex vivo* fat property measurements, it should still be much less lossy than high-water-content tissues, making microwave signal propagation readily feasible over 10 cm of breast tissue. Third, the breast presents a small volume that is easily accessible, making it a far more tractable site for effective microwave imaging than larger, more general, anatomical areas, such as the abdomen or pelvis.

As a result, breast imaging is particularly attractive for exploring many of the emerging concepts of near-field model-based imaging with active microwave illumination, which, to date, have been largely demonstrated in theory [32]–[35], although important laboratory developments have also now appeared [36]–[39]. A recent series of studies by Hagness *et al.* [40], [41] nicely illustrates the opportunities for active microwave sensing in the breast. They simulate the ability to exploit ultrawide-band microwave radar technology in a confocal topology to detect millimeter-sized lesions at considerable depths from the tissue surface using powerful finite-difference time-domain (FDTD) computational analysis. Following a similar approach, Fear and Stuchly have introduced a microwave-breast-imaging technique that is more suitable to clinical implementation [42]. These results are encouraging and further support the notion that microwave breast imaging should be aggressively pursued in a variety of forms.

Motivated by the overall needs to improve breast cancer detection and characterization and our standing interest in advancing medical microwave imaging, we have developed a prototype microwave tomographic breast scanner operating over the frequency band of 300–1000 MHz. The prototype is an adaptation of a previously reported laboratory-scale system where we have modified the antenna array structure to produce multiple two-dimensional (2-D) images beginning near the chest wall and extending anteriorly past the nipple. Exams are delivered conveniently and comfortably without compression in the prone position with the breast pendant in a coupling fluid. The results reported here indicate that we are able to sense variations in tissue content (generally, fat versus higher water content constituents) that are consistent with the medical histories of the participants examined to date. The images produced in this limited pilot series of clinical encounters display considerable consistency between breasts of a particular individual. Interestingly, the average recovered permittivity values appear to vary from patient to patient, but correlate with radiographic density categorization and are often significantly greater than those reported in *ex vivo* studies [29], [30]. The images shown here appear to result from the first use of active near-field microwave data acquisition coupled to model-based image reconstruction methodology to produce *in vivo* electromagnetic property exams of the breast. In this sense, these initial results are very exciting and encouraging. They also suggest new areas of study, which will be critical to the overall development of microwave breast examination.

## II. Methods

### A. Data Acquisition System

We have developed a data acquisition system (with up to 32 channels) that can be employed with a fixed array of antennas (Fig. 1) [38], [43]. The hardware has been designed to have each antenna operate in either transmit or receive mode in order to maximize the amount of measurement data that can be recorded while maintaining a channel-to-channel isolation of greater than 120 dB and an overall linear dynamic range of 130 dB. Monopole antennas have been chosen as the radiating elements for several important reasons. First, the monopole can be effectively modeled as a line source in a 2-D imaging problem [43]. In terms of the data–model match between the physics of the microwave illumination and the numerical model (the best match producing the highest quality images [37]–[39]), we have found the monopole to be the simplest element to represent accurately. Second, although the monopole antenna typically exhibits undesirable characteristics when operating in a lossless medium (narrow bandwidth and excitation of surface waves), it is an excellent radiator in a lossy environment where resistive loading substantially increases the usable bandwidth with no perceptible excitation of surface currents [43]. Through incorporation of a heterodyning modulation scheme, a 200-kHz A/D board and signal phase and amplitude extraction in software, data acquisition time has been reduced to a few seconds for a complete measurement set at each frequency. The system has been consolidated onto a single cart for portability and ease of connection to a clinical interface for delivery of breast exams [see Fig. 1(c)].

This new prototype has facilitated the study of key issues related to near-field 2-D microwave imaging with a fixed antenna array including the influence of its nonactive members. We have found it important to model each nonactive antenna as a microwave sink so that entering signals are absorbed and not re-ra-

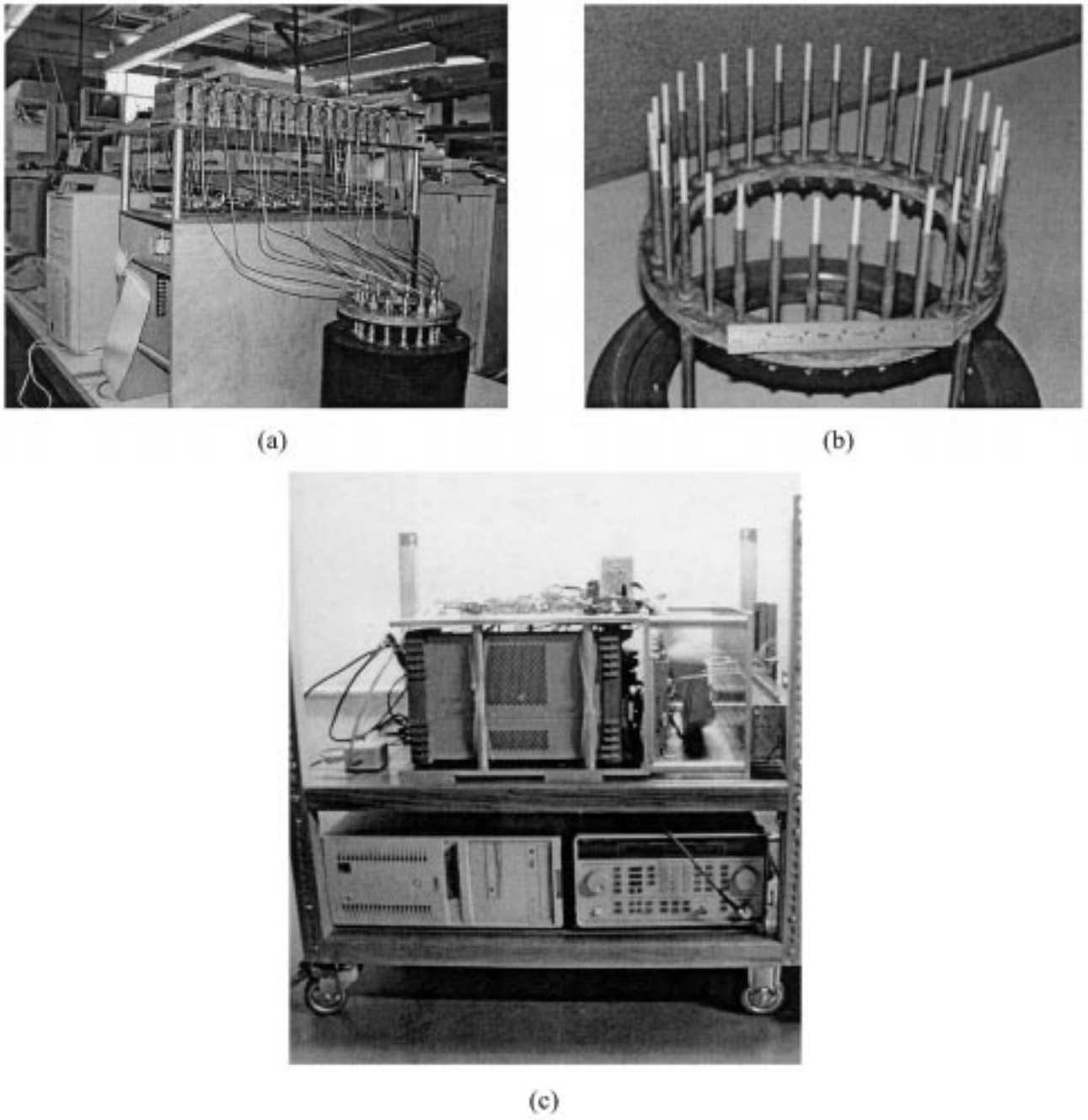


Fig. 1. Prototype imaging system. (a) Tank with the 32-channel data acquisition system connected and in laboratory scale operational mode. (b) View of a 32-antenna array suspended from the positioning plate (no saline in tank). (c) View of the data acquisition system mounted on a cart—including microwave source, power supplies, function generator, Dell 300-MHz PC, and complete microwave switching, receiver, and modulation circuitry.

diated [38], [44]. This has been accomplished in the numerical model by imposing an impedance boundary condition on a finite diameter about each nonactive element. The radius of the circle of influence and the impedance chosen at its boundary have been derived empirically from measured data. In terms of the hardware, we have selected matched switches as the last components in the switching matrix such that when an antenna is in the nonactive state, any coupled signal is transmitted via a coaxial cable to the switch and terminated without being re-radiated. Significant image quality improvements have been achieved with this implementation.

### *B. Water-Coupled Clinical Interface*

We have designed and constructed a prototype breast imaging interface whose most significant features are illustrated in Fig. 2. Given that we successfully achieved a number of important milestones with our laboratory system in terms of demonstrating practical imaging using experimental data, we elected to modify our tank design as the most viable option for realizing a near-term microwave approach to breast imaging. The major challenge in adapting the laboratory system has been the requirement that the cables and associated electrical connections be maintained in a dry environment while the

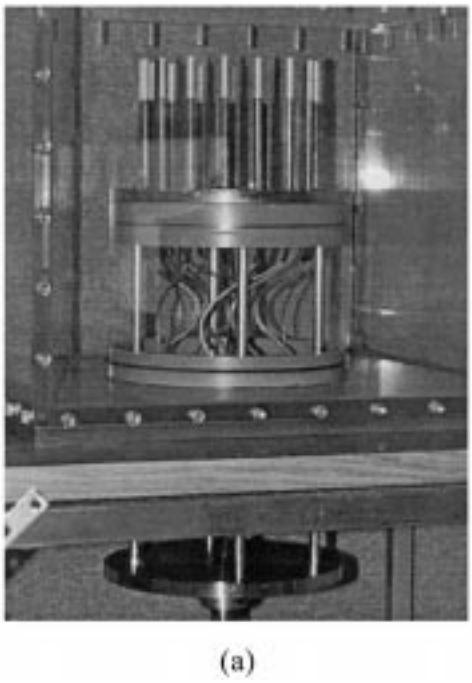

(a)

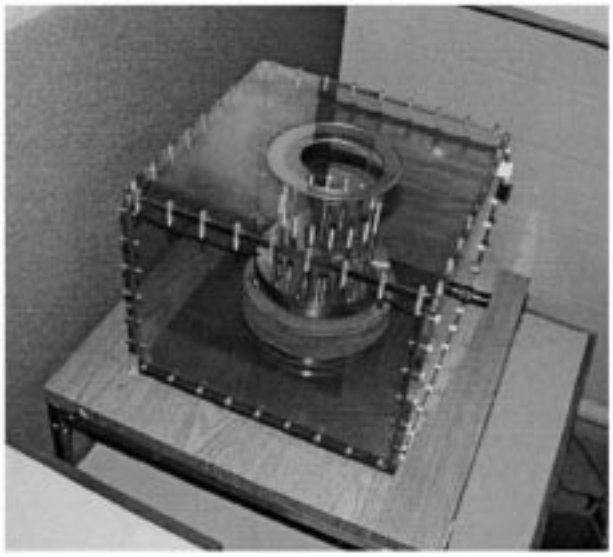

(b)

Fig. 2. Illumination tank (water removed for illustration). (a) Antenna array showing internal cable connections with the bellows removed (array is in lowered position). (b) Top view showing aperture for breast with antenna array below and bellows in place to shield electronics.

antennas are submerged in a saline bath. This constraint has also been motivated by the fact that an attractive clinical exam position has the subject lie on a table above the tank with her breast pendant in a coupling fluid. As a result, it became necessary to devise an interface with the radiating monopole antennas oriented upwards to allow for illumination of the breast as close to the chest wall as possible. This required that the antennas protrude through the middle of the tank (with the radiating elements surrounding the breast on a 15-cm diameter) and their associated connectors and cables originate from below the tank, yet be shielded from the saline bath. Accomplishing this design allows the antenna array to be easily connected to the existing microwave data acquisition system, making the clinical interface act as an individual modular unit. We have also incorporated the capability of raising and lowering the antenna array through the mechanical motion of a hydraulic jack located below the array housing, thus providing multislice illumination of the breast. Flexible cables allow vertical motion of the antenna array with respect to the fixed connector bulkhead underneath the tank, thereby yielding minimal variation in the measured fields due to cable flexing and bending (see Fig. 2). The shielding of the microwave components from the saline bath has been realized with a cylindrical bellows, which can withstand the water pressure in both its compressed and uncompressed states without leaking. A simple pumping mechanism attached to a reservoir tank (not shown) has also been implemented for rapidly maintaining a set water level during a clinical session.

Fig. 3. Fully assembled clinical microwave imaging system with the sheets raised to show microwave electronics and tank overflow reservoir located below the table.

Fig. 3 shows the fully integrated system as it exists in the clinical setting. The data acquisition and illumination tank modules are connected to form the examination table. The space underneath the table is used to house the saline overflow reservoir. Padding the table with a thin air mattress and pillows improves patient comfort. The electronics are controlled remotely from the adjacent room to maximize patient privacy and an exam assistant remains with the patient throughout the session to help with breast positioning and getting on and off the table.

### *C. Phantom Electrical Property Measurement*

In order to investigate the electrical properties of liquids with values roughly equivalent to breast tissue and their variation with increasing water content, it is important to have a well-controlled measurement system. In this paper, we have employed an HP85070B Dielectric Probe Kit in conjunction with an HP 8753C Network Analyzer where the actual testing and calibration is controlled by a Dell Dimension 466V PC. Calibration of

the probe is performed with the following three known termination standards:

1) air;
2) shorting block;
3) 25 °C water.

In general, the measured values have been repeatable to within 1%.

### *D. Clinical Examination Protocol*

Women participated in these breast exams under informed consent approved by the Institutional Review Board, Dartmouth College, Hanover, NH, for the protection of human subjects. Having completed the consent-form process, participants were fitted with a sizing ring, which stabilized the breast in the center of the antenna array during imaging. Women were then assisted on to the microwave exam couch and positioned prone with the breast to be imaged pendant in the coupling fluid. Special attention was given to getting as much of the breast tissue in the axilla area into the imaging array as possible. The coupling fluid was 0.9% saline prepared the day before each session to allow for temperature equilibration. Fresh saline batches were used in each exam. Initially, the water level was lower than needed in order to prevent overflow as the breast was positioned for the exam. Once in position, the antenna array was elevated to its nearest point to the chest wall and a circulating pump connected to a saline reservoir raised the water level to cover the antenna tips. Data acquisition ensued for each antenna array position and consisted of complete tomographic data (16 antenna excitations and associated measurements) for seven frequencies recorded in approximately 90 s. The antenna array was then lowered in regular increments (typically 1 cm) based on a scale fixed to the side of the water tank. At each new antenna array position, the water volume was adjusted to maintain a constant level throughout the exam and a complete set of multispectral microwave-imaging measurements was recorded. The entire process generally consisted of seven separate data acquisition levels (i.e., antenna-array heights), which were completed in approximately 10–15 min per breast (including breast and array positioning time). Where appropriate, the contralateral breast was also examined. Fig. 4 shows a photograph of an exam in session and a close-up view of the breast in position within the tank centered in the antenna array.

Immediately prior to each exam, a full system calibration was performed. This consisted of collecting measurements for each transceiver position and detector site within a complete image reconstruction data set for each antenna-array level to be used during the exam at the anticipated water level in the tank, but with no heterogeneity (i.e., breast) located within the array. This data was then used to calibrate the measured responses from the breast using the procedures identified in [37]. For the exams reported here, an air interface existed at the aperture opening in the examination table during calibration. No attempt has been made to compensate for the fact that the chest wall covers this opening during examination. Future calibrations may be well advised to place a saline bag over the aperture opening to mimic the presence of the body.

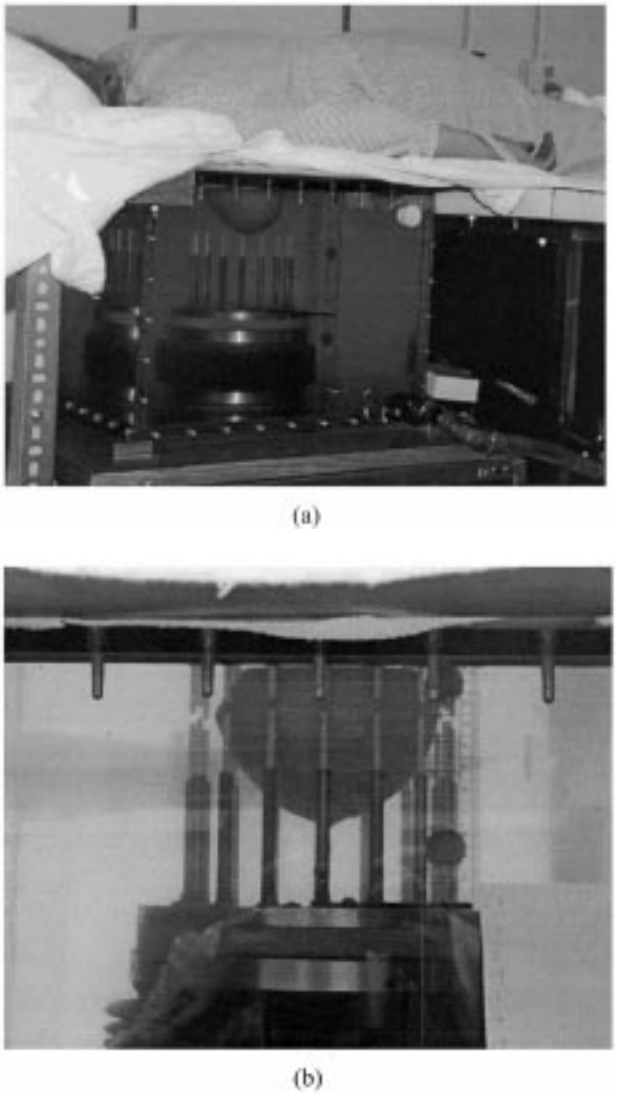


Fig. 4. Photographs of a microwave exam in session. (a) Close-up view. (b) The breast in position within the center of the antenna array.

## III. Results

An initial set of microwave-breast-imaging examinations have been performed on five volunteers using the prototype system described in Section II. All subjects had received recent mammograms and presented with no abnormalities that would be considered suspicious at the time of these microwave exams. Two of the women had undergone previous surgeries on the imaged breasts—a breast reduction and lumpectomy. Participants ranged in age from 48 to 76 and were all post menopause with none receiving estrogen replacement therapy. Two of the five had a prior mastectomy on one breast. There was a mixture of radiographical breast density ratings in the study and a considerable range in breast size from patient to patient. The results reported here focus on 900-MHz scans, although data was recorded for frequencies ranging from 300 to 900 MHz in 100-MHz increments. The background medium used to couple the microwave signals into the breast had nominal relative permittivity and conductivity values of

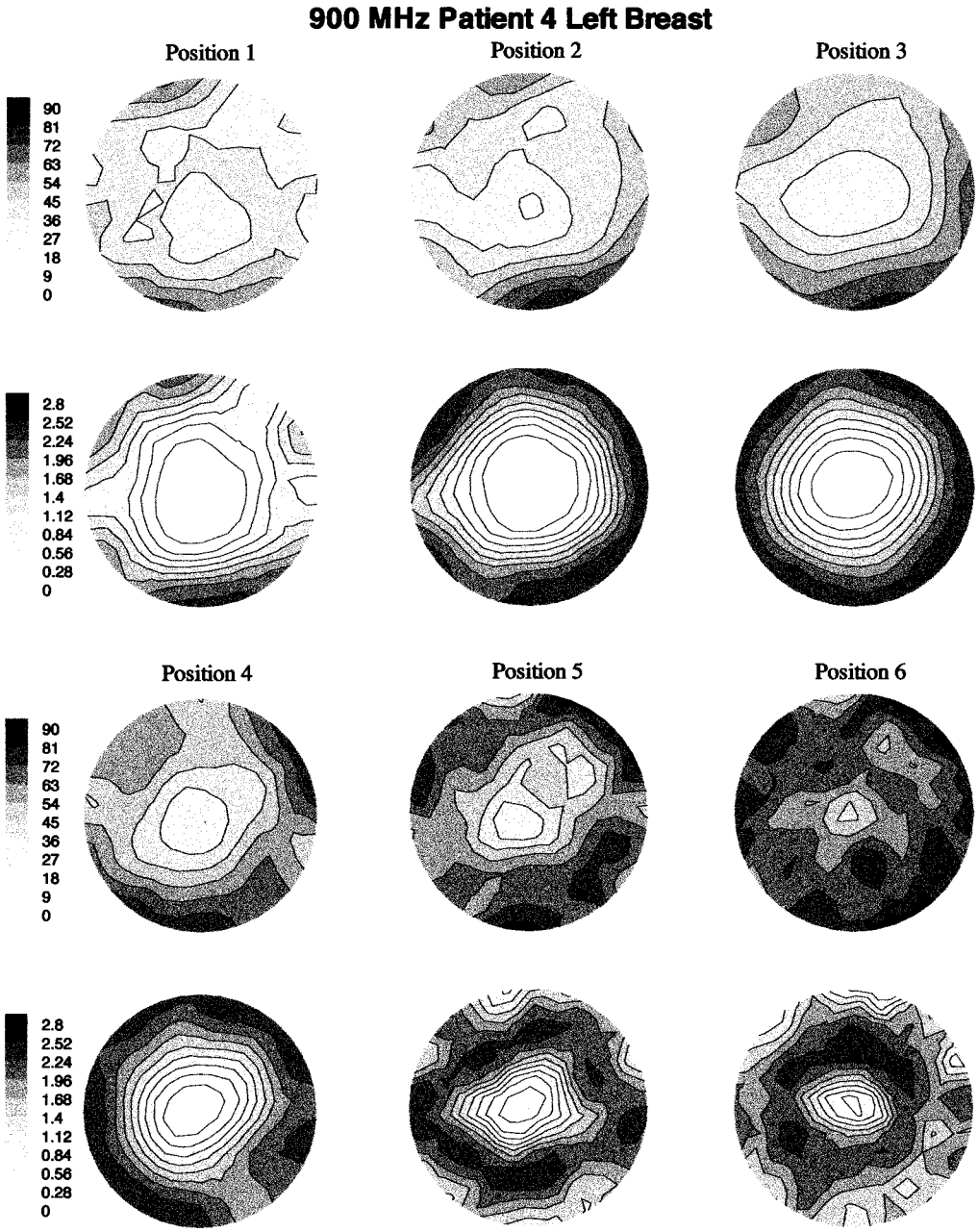


(a)

Fig. 5. Recovered 900-MHz relative permittivity and conductivity images for: (a) left-hand-side breasts of Patient 4. Images are displayed for all vertical positions where the breast intersects the imaging plane—in this case, positions 1–6.

79.0 and 1.86 (siemens/meter), respectively. Images presented here are in standard en face radiological view. For the purposes of this paper, we have differentiated a large (from a small) breast as one which extends to at least the fifth vertical array position from the chest wall. This designation is important for our prototype system because smaller breasts present a more difficult imaging situation due to the fact that fewer imaging slices can be obtained and these are located closer to the surface of the tank where artifacts from wave reflections at the water, air, patient, and tank interfaces are more problematic at the present time. All images were formed using our iterative reconstruction algorithm in roughly 20 min (ten iterations) on an IBM RS6000 model 260 workstation.

### *A. Large Asymptomatic Contralateral Breast Comparison*

Fig. 5(a) and (b) illustrates the recovered images (paired as relative permittivity $\varepsilon_r$ and conductivity $\sigma$) at six array positions for both the left- and right-hand-side breasts of Patient 4. This patient was 49 years old and her breasts were categorized as radiographically dense by the reading radiologist. It should be noted that the background (0.9% saline) has considerably higher permittivity and conductivity than those values recovered within the breast and this contrast contributes to the shading of the surrounding regions and the steep gradient associated with the boundary between the saline and breast. The $\sigma$ images of the breasts display uniform circularly symmetric low-conductivity regions of diminishing diameter for slices further from the chest

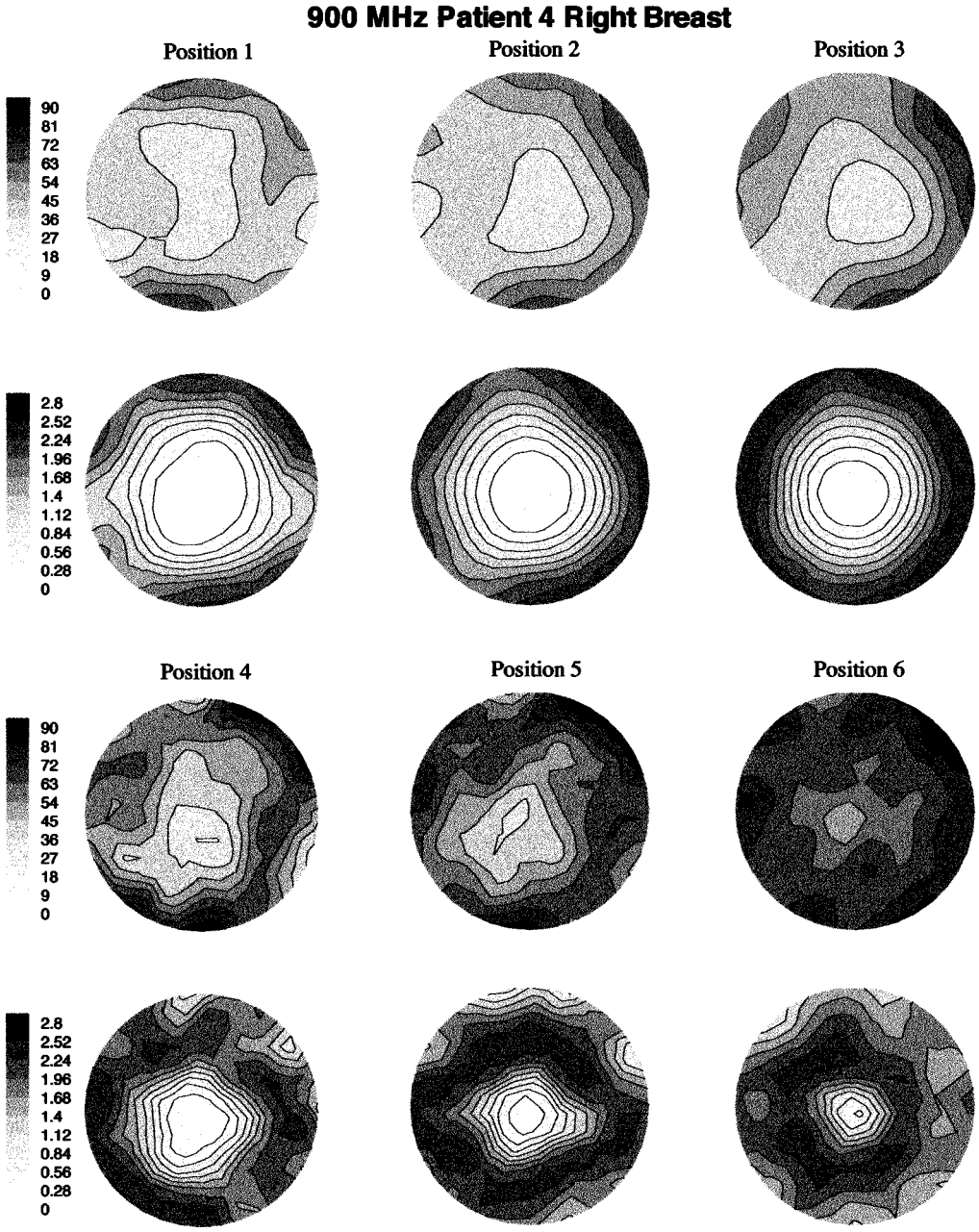


(b)

Fig. 5. *(Continued.)* Recovered 900-MHz relative permittivity and conductivity images for: (b) right-hand-side breasts of Patient 4. Images are displayed for all vertical positions where the breast intersects the imaging plane—in this case, positions 1–6.

wall corresponding to the natural breast geometry. The relative permittivity images generally display more complex geometric variation, especially with respect to delineation of the breast surface for the two imaging planes closest to the chest wall where some of the variation may be due to the out-of-plane influence of the chest wall and the mild deformation of the breast as it presses against the aperture in the table above the saline tank. Nonetheless, the average relative permittivity over each slice appears to be quite uniform and consistent from slice to slice and breast to breast. The mean values of $\varepsilon_r$ for the left- and right-hand-side breasts were 35.4 and 36.2 with standard deviations of 3.9 and 3.6, respectively (Note that the actual boundary of the breasts over which the analyses were performed were drawn to minimize the influence of the steep boundary gradients, but include the largest possible area of breast tissue). These relative permittivity values are considerably higher than those reported in the literature for *ex vivo* studies (typically ranging between 15–20 for 300–900 MHz [29]). Similarly to the relative permittivity, the conductivity values were also consistent between both breasts. Means and standard deviations for both electromagnetic quantities are summarized in Table I for all five study participants.

### *B. Small Asymptomatic Contralateral Breast Comparison*

Fig. 6(a) and (b) illustrates the recovered images for both the left- and right-hand-side breasts at three vertical array locations for Patient 2. This patient was 57 years old and her breasts were

TABLE I
MEAN AND STANDARD DEVIATION OF RECOVERED RELATIVE PERMITTIVITY AND CONDUCTIVITY VALUES OF BREASTS FOR PATIENTS 1–5

| Patient | | | Left | | | | Right | | | |
|---|---|---|---|---|---|---|---|---|---|---|
| | | | $\varepsilon_r$ | | $\sigma$ (siemens/m) | | $\varepsilon_r$ | | $\sigma$ (siemens/m) | |
| | Age | Breast Density* | Mean | STD | Mean | STD | Mean | STD | Mean | STD |
| 1 | 76 | ft | 17.22 | 11.21 | .5892 | .3547 | 20.90 | 12.09 | .6390 | .3498 |
| 2 | 57 | ft | 31.14 | 4.35 | .6902 | .3650 | 31.88 | 5.18 | .6286 | .3581 |
| 3 | 52 | hd | 36.44 | 6.24 | .6869 | .3156 | | | | |
| 4 | 49 | dn | 35.43 | 3.93 | .5943 | .3841 | 36.18 | 3.61 | .6127 | .4011 |
| 5 | 48 | sc | 30.85 | 7.22 | .6350 | .3550 | | | | |

*Radiographic density definitions: ft = fatty, sc = scattered, hd = heterogeneously dense and dn = dense.

considered radiographically fatty by the reading radiologist. It is evident from these images that the breasts for this patient are smaller both in terms of the diameters recovered at each vertical position and the disappearance of the breast after the third movement of the antenna array away from the chest wall. Similarly to Patient 4, there is a noticeable level of consistency between each breast in shape and size. The relative permittivity values are fairly uniform over each breast with the average between the two sides agreeing quite well: $\varepsilon_r = 31.1 \pm 4.4$ for the left-hand-side breast and $\varepsilon_r = 31.9 \pm 5.2$ for the right-hand-side breast. These quantities are slightly lower than those for Patient 4 who was assessed in the radiologically dense category. As with Patient 4, the size of the breast appears to be larger when comparing the $\varepsilon_r$ images to the $\sigma$ images. There also appears to be fewer artifacts in the perimeter of the relative permittivity images for the antenna array positions closest to the chest wall compared to Patient 4, presumably because the smaller breast experiences less tissue deformation when pressed against the tank aperture.

### C. Breast Reduction Surgery

Fig. 7 illustrates the recovered images for the left-hand-side breast at three vertical array positions for Patient 3 (right-hand-side breast had undergone a mastectomy several years prior to this exam). This patient was 52 years old and her breast was categorized radiographically as heterogeneously dense. She had breast-reduction surgery performed on her left-hand-side breast with the tissue removed below the nipple in the en face view. The intent of these procedures is usually to remove fatty tissues while sparing as much of the glandular, muscle, and nerve constituents as possible. The $\varepsilon_r$ images clearly show a ring of relatively low permittivity about the outer perimeter of the breast with a gap (as indicated by the higher permittivity replacement zone) in the lower portion of the image toward the left-hand side of center. From general anatomy [45]–[48], the breast is considered to be a relatively homogeneous tissue within its central most region, but with a varying thickness layer of subcutaneous fat completely surrounding the periphery. From *ex vivo* data, the fat will tend to have lower relative permittivity values ($\varepsilon_r \approx 5$) than those of the mammary glands (ranging from 15 to 20). Had this surgery not been performed, it would be reasonable to expect the appearance of a low-permittivity ring about the entire breast. Initial experience indicates that this ring of low dielectric does not always appear (presumably due to an electrically thin subcutaneous fat layer) and may vary in accentuated cases where the layer is both thicker in size and lower in its recovered permittivity value. While the orientation of the reduction surgery does not perfectly align with the localized permittivity increase in the recovered images, uneven tissue replacement after surgery and registration inaccuracies in breast positioning during imaging in the array could easily explain these differences.

### D. Contralateral Breast Comparison—Left-Hand-Side Breast Lumpectomy

Fig. 8(a) and (b) shows the recovered images for both the left- and right-hand-side breasts at three vertical locations for Patient 1. This woman was 76 years old and her breasts were considered radiographically fatty by the reading radiologist. She previously had lumps removed from her left-hand-side breast. The $\varepsilon_r$ images for the first two positions of the right-hand-side breast present relatively thick rings of low-permittivity material surrounding central regions of considerably higher values. Presumably the outer rings coincide with a thick layer predominantly composed of fat and a central zone containing a higher proportion of mammary glands. By the third position, the diameter of the breast is sufficiently small that the imaging technique is unable to spatially distinguish between these zones and the resulting image appears as a single large low-permittivity region. Images from the left-hand-side breast are also quite instructive. Where there was a continuous ring about the right-hand-side breast in the second vertical position, there is a distinct gap in the ring for the left-hand-side breast. This coincides well with the location of the scar from where the lumps were previously removed by surgery. Presumably portions of the fat invaded by the surgical procedure were replaced by scar and shifting mammary tissue to produce higher permittivity values more consistent with mammary and higher water-content components. As

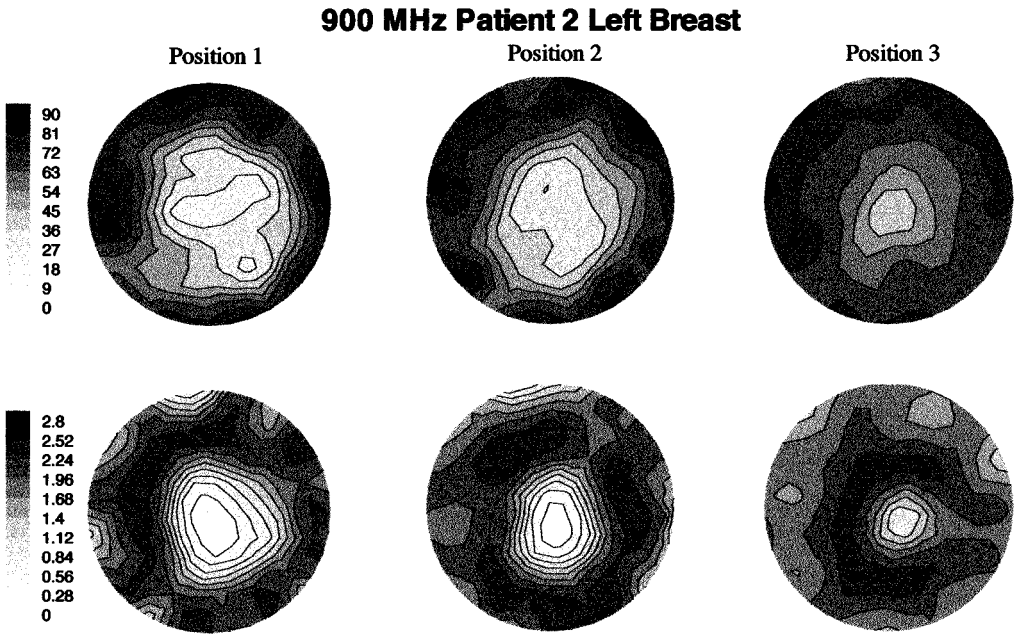


(a)

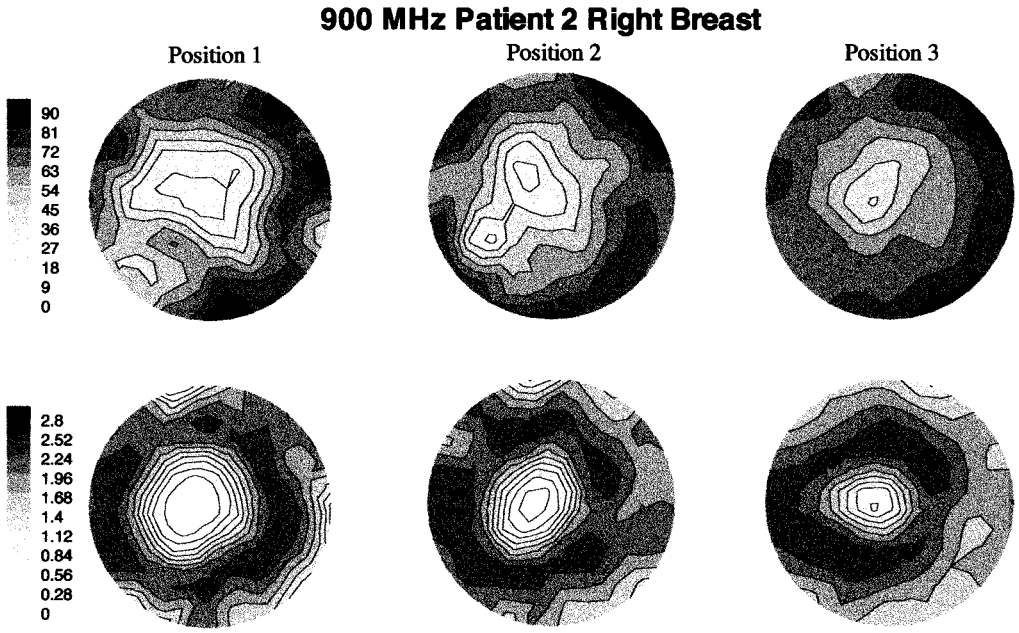


(b)

Fig. 6. Recovered 900-MHz relative permittivity and conductivity images for both: (a) left- and (b) right-hand-side breasts of Patient 2. Images are displayed for all vertical positions where the breast intersects the imaging plane—in this case, positions 1–3.

shown in Table I, the average permittivity values for Patient 1 were considerably lower than for the other four subjects.

### *E. Mean Tissue Permittivity Values*

Table I shows the mean and standard deviation of the relative permittivity and conductivity for the five women imaged in this pilot study. These values were produced by first transforming each image to grayscale, selecting a representative perimeter of the breast using the National Institutes of Health (NIH) Image 1.61 and applying the accompanying analysis tools to determine the relative statistics. The final grayscale values were then easily transformed back to the relative permittivity and conductivity scales. Given that the reported mammary permittivity values in the Joines [29] *ex vivo* study were roughly 15 at 900 MHz, the values we have recovered are considerably higher. Excluding Patient 1, who was considerably older than the others, there appears to be the suggestion of a correlation between the radiographic density and the average recovered permittivity values. Subjects 2 and 5 were categorized radiologically as fatty and scattered (implying high fat content) and had corresponding permittivity averages of approximately 31, whereas Subjects 3 and 4 were characterized as heterogeneously dense and dense (implying less fat) and had average permittivities in the 35–36

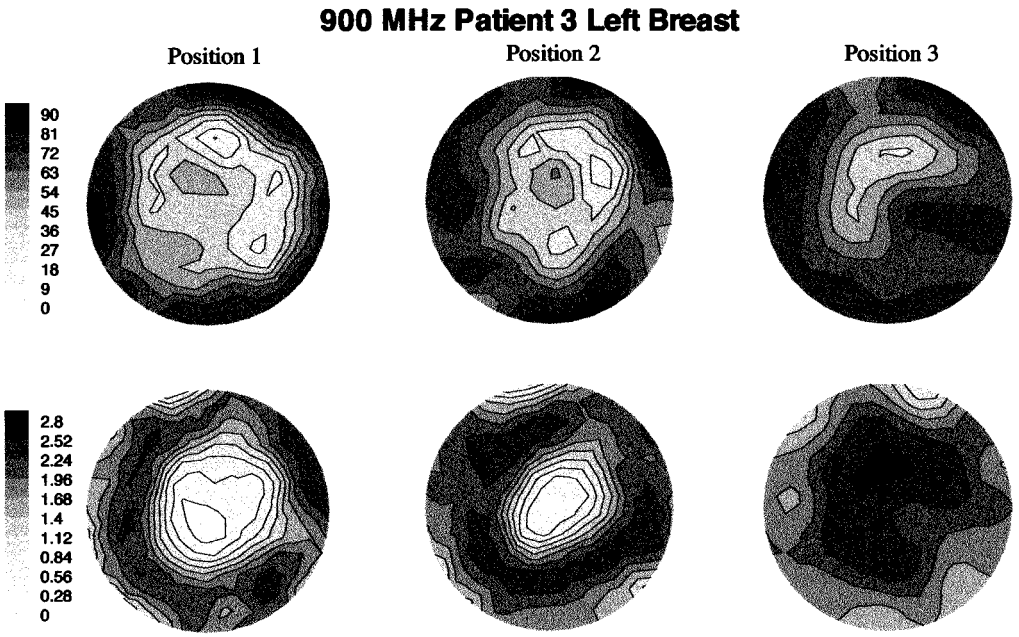


Fig. 7. Recovered 900-MHz relative permittivity and conductivity images for the left-hand-side breast of Patient 3. Images are displayed for all vertical positions where the breast intersects the imaging plane—in this case, positions 1–3.

range. Thus, it appears that the lower permittivity averages correspond to higher breast fat content, as would be expected. Subject 1 had considerably lower permittivity values (average less than 20), which may reflect the progressive atrophying of glandular tissue and subsequent replacement with fat with increasing age after menopause. In general, the trend toward higher mean-permittivity values relative to those from *ex vivo* measurements is most likely the result of tissue perfusion. The presence of even small quantities of water well mixed with low-permittivity materials can have a disproportionately large effect on the overall electrical properties. Fig. 9 shows plots of the relative permittivity for water mixed with corn syrup as a function of mixture proportion at several frequencies. (The relative permittivity of corn syrup without water is quite close to the *ex vivo* values for mammary tissue.) Increasing the ratio of water to syrup from 0 to 1 : 5 at 900 MHz raises the relative permittivity from 19.8 to 33.3. Most likely, the presence of the highly polar water molecules is driving this effect.

## IV. Discussion

A clinical water-coupled prototype microwave-breast-imaging system has been developed to perform multislice examinations of the breast over a broad frequency range. The exam sessions have generally been short (≈10–15 min per breast for seven slices and seven frequencies per slice) and well tolerated by the study participants. Several important observations can be made with regard to these initial clinical encounters. First, this experience suggests that the relative permittivity values for the breast measured *in vivo* are considerably higher than those recorded during *ex vivo* experiments, which is an important finding that needs to be confirmed because it may impact future system design. From the imaging point-of-view, it is desirable that the coupling medium be matched to the tissue under study. High coupling medium contrast could potentially compromise the ability to image internal structures and abnormalities due to the large reflections that would occur at the breast surface. Saline was used here because of its availability and low cost, but its high relative permittivity is in considerable contrast with published *ex vivo* mammary tissue values. Nonetheless, these initial clinical investigations indicate that informative images can be produced in a saline coupling medium despite its contrast with the breast in part because the *in vivo* permittivity values of the breast may be considerably higher and possess greater heterogeneity than originally anticipated. These results suggest further investigation is necessary and it is likely that a more optimally selected coupling fluid will be important in the future.

In addition to contrast issues at the interface of the breast and liquid coupling medium, the possibility of normal breast tissue having higher permittivity properties than previously reported in *ex vivo* studies may have important implications for microwave breast cancer detection. Specifically, if the normal breast has an average $\varepsilon_r$ of 30–36 at 900 MHz compared to the previously assumed level near 15, its contrast with respect to a malignant lesion having an $\varepsilon_r$ in the range of 50–70 will be reduced. The potential for very high contrast has been a key driver in the appeal of this modality and it may not be as great as initially anticipated, although even 2 : 1 tumor to normal tissue contrast is not insignificant when compared to the few percent that exists in many traditional imaging settings.

At the current stage of understanding, it is difficult to estimate the spatial resolution evident in the *in vivo* breast images reported here. Property variations that are on a spatial scale of a centimeter or less occur, although larger zones of homogeneity also appear. Since resolution can only be properly evaluated in terms of contrast and the electromagnetic property heterogeneity within the breast *in vivo* is not well characterized at this

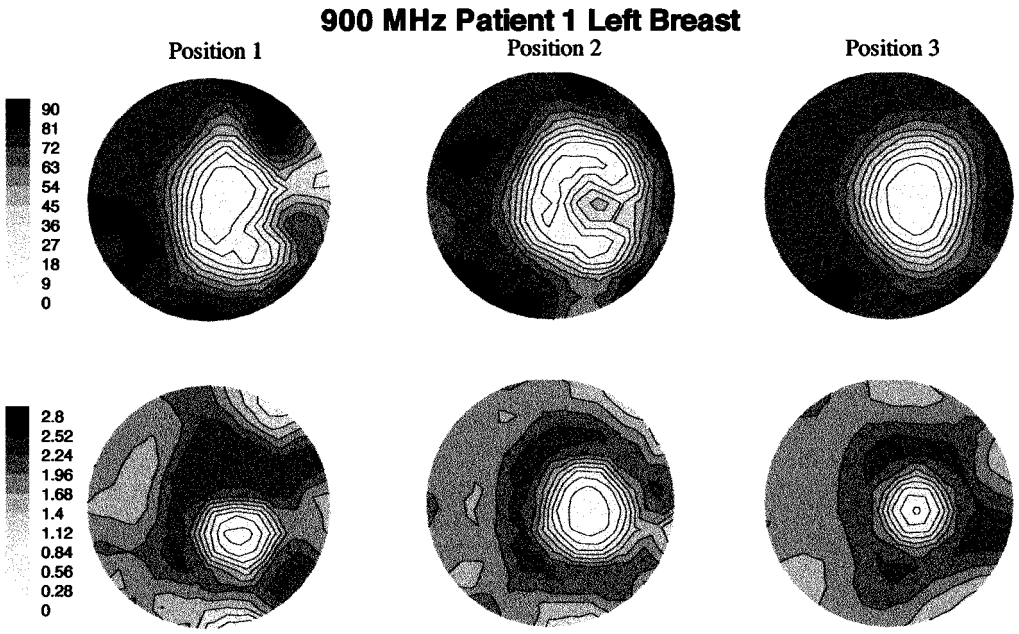


(a)

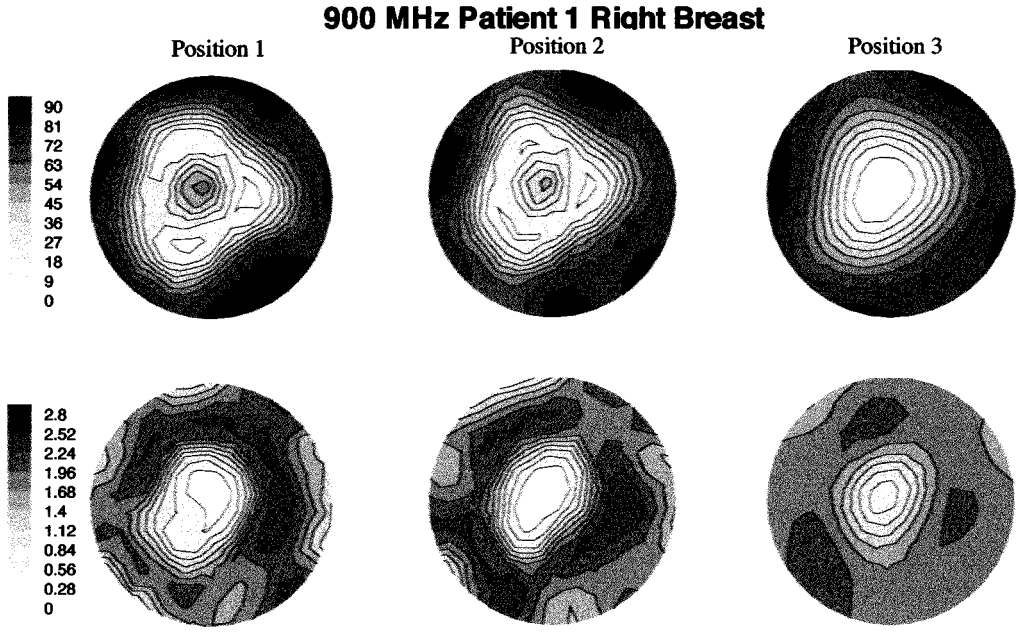


(b)

Fig. 8. Recovered 900-MHz relative permittivity and conductivity images for both: (a) left- and (b) right-hand-side breasts of Patient 1. Images are displayed for all vertical positions where the breast intersects the imaging plane—in this case, positions 1–3.

time, meaningful quantification of the spatial resolution of these breast images cannot been completed. Based on past laboratory experience, our system has consistently demonstrated a spatial resolution of 1 cm in both single and multitarget phantom experiments utilizing operating frequencies in the range of 500–900 MHz [37], [39]. High-contrast structures as small as 0.4 cm have been evident as well [37]. These findings are in line with published results for near-field imaging approaches where the spatial resolution is limited by signal-to-noise and not the half-wavelength typically associated with diffraction limited techniques [36], [49]–[54]. More challenging imaging studies [38] where varying diameter tubes of saline were inserted into 8.2-cm-diameter cylinders of freshly excised breast tissue recovered from reduction surgeries have shown that 1-cm saline inclusions were generally visible only in the permittivity part of the image at low frequencies. As the operating frequency increased from 500 to 900 MHz, perturbations in the conductivity component were also evident. Similarly, the conductivity images from these patient examinations identify the breast surface quite well with the internal conductivity appearing relatively low and homogeneous. Hence, we expect improvements in terms of detecting heterogeneities within the patient conductivity images with increased operating frequency. The goal for the next-generation system is to operate from 500 MHz

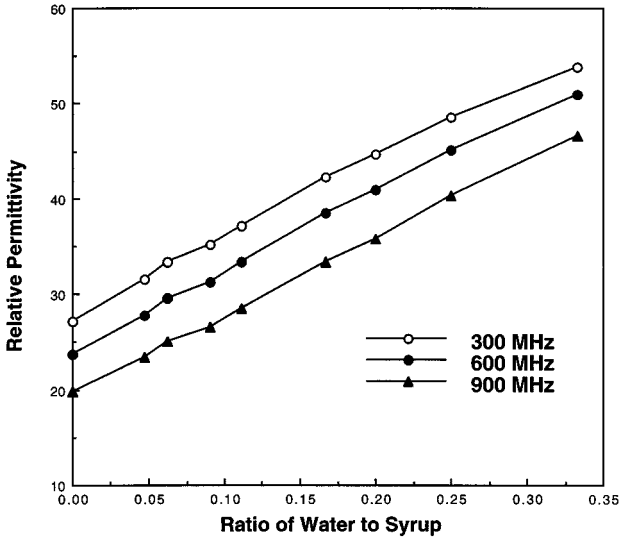


Fig. 9. Plot of the relative permittivity of water/syrup mixtures as a function of the water-to-syrup ratio.

to 3 GHz. Nonetheless, the recovered permittivity images for the participants examined to date show that our imaging system can detect subtle tissue abnormalities, including alterations due to surgical procedures such as lumpectomies and breast reductions. These results suggest that recovery of electrical properties may provide useful diagnostic information about tissue abnormalities.

## V. Conclusions

A prototype microwave breast scanner has been realized. Breast exams delivered through water coupling to the pendant breast with the participant positioned prone on an examination table has been found to be a practical comfortable approach to microwave breast imaging. This clinical experience appears to be the first report of active near-field microwave imaging of the breast where model-based image reconstruction methodology has been deployed to convert the measured microwave signals into spatial maps of electrical permittivity and conductivity. While certainly preliminary, the results are encouraging and have already supplied some interesting findings. Specifically, it appears that the average relative permittivity of the breast as a whole may correlate with radiological breast density categorization and may be considerably higher than previously published values, which have been based on *ex vivo* tissue specimens. Clearly, a considerable amount of additional experience is needed with microwave imaging of both the normal and abnormal breast before any conclusions can be reached about the diagnostic value of microwave imaging in this setting.

## References

[1] L. A. G. Rise *et al.*, "SEER cancer statistics review 1973–1994," Nat. Cancer Inst., Bethesda, MD, NIH Pub. 97-2789.

[2] M. Brown, F. Houn, E. Sickles, and L. Kessler, "Screening mammography in community practice," *Amer. J. Roentgen.*, vol. 165, pp. 1373–1377, 1995.

[3] J. G. Elmore *et al.*, "Ten year risk of false positive screening mammograms and clinical breast examinations," *New Eng. J. Med.*, vol. 338, pp. 1089–1096, 1998.

[4] R. Rosenberg *et al.*, "The New Mexico mammography project screening mammography performance in Albuquerque, New Mexico 1991–1993," *Cancer 1996*, vol. 78, pp. 1731–1739, 1996.

[5] P. T. Huynh, A. M. Jarolimek, and S. Daye, "The false-negative mammogram," *Radiograph.*, vol. 18, no. 5, pp. 1137–1154, 1998.

[6] R. D. Rosenberg, W. C. Hunt, M. R. Williamson, F. D. Gilliland, P. W. Wiest, C. A. Kelsey, C. R. Key, and M. N. Linver, "Effects of age, breast density, ethnicity, and estrogen replacement therapy on screening mammographic sensitivity and cancer stage at diagnosis: Review of 183 134 screening mammograms in Albuquerque, New Mexico," *Radiology*, vol. 209, no. 2, pp. 511–518, 1998.

[7] M. Laya, E. Larson, S. Taplin, and E. White, "Effect of estrogen replacement therapy on the specificity and sensitivity of screening mammography," *J. Nat. Cancer Inst.*, vol. 88, pp. 643–649, 1996.

[8] V. P. Jackson *et al.*, "Imaging of the radiographically dense breast," *Radiology*, vol. 188, pp. 297–301, 1993.

[9] N. F. Boyd *et al.*, "Quantitative classification of mammographic densities and breast cancer risk," *J. Nat. Cancer Inst.*, vol. 87, pp. 670–675, 1995.

[10] J. N. Wolfe, "Breast parenchymal patterns and their changes with age," *Radiology*, vol. 121, pp. 545–552, 1976.

[11] J. Brisson *et al.*, "The relation of mammographic features of the breast to breast cancer risk factors," *Amer. J. Epidemiol.*, vol. 115, pp. 438–443, 1982.

[12] O. Am and N. F. Boyd, "Mammographic parenchymal patterns: A marker of breast cancer risk," *Epidemiol. Rev.*, vol. 15, pp. 196–208, 1993.

[13] I. T. Gram *et al.*, "Reproductive and menstrual factors in relation to mammographic parenchymal patterns among perimenopausal women," *Br. J. Cancer*, vol. 71, pp. 647–650, 1995.

[14] P. C. Stomper, D. J. D'Souza, P. A. DiNitto, and M. A. Arredondo, "Analysis of parenchymal density on mammograms in 1353 women 25–79 years old," *Amer. J. Roentgen.*, vol. 167, pp. 1261–1265, 1996.

[15] J. Elmore *et al.*, "Variability in radiologists' interpretations of mammograms," *New Eng. J. Med.*, vol. 331, pp. 1493–1499, 1994.

[16] C. Beam, P. Layde, and D. Sullivan, "Variability in the interpretation of screening mammograms by US radiologists," *Arch. Internal. Med.*, vol. 156, pp. 209–212, 1996.

[17] D. B. Kopans, *Breast Imaging*. Philadelphia, PA: J. B. Lippincott, 1989, pp. 14–15.

[18] G. Piperno, E. H. Frei, and M. Moshitzky, "Breast cancer screening by impedance measurements," *Frontiers Med. Biol. Eng.*, vol. 2, no. 2, pp. 111–117, 1990.

[19] J. Cuzick, R. Holland, V. Barth, R. Davies, M. Faupel, I. Fentiman, H. J. Frischbier, J. L. LaMarque, M. Morgan, V. Sacchini, D. Vanel, and U. Veronesi, "Electropotential measurements as a new diagnostic modality for breast cancer," *Lancet*, vol. 352, pp. 359–363, 1998.

[20] S. I. Fields *et al.*, "Adjunctive improvement of mammographic accuracy using electrical impedance scanning," RSNA, Chicago, IL, Abstract, Nov. 1998.

[21] J. Shaeffer, K. L. Carr, L. A. O'Grady, and A. Resciniti, "ONCOSCAN combined with mammography to determine breast biopsy," in *European Congr. Radiol.*, Vienna, Austria, Mar. 7–12, 1999.

[22] J. R. Keyserlingk, P. D. Ahlgren, E. Yu, and N. Belliveau, "Infrared imaging of the breast: Initial reappraisal using high-resolution digital technology in 100 successive cases of stage I and II breast cancer," *Breast J.*, vol. 4, no. 4, pp. 245–251, 1998.

[23] R. I. Elliot and J. F. Head, "Thermography: Its relation to pathologic characteristics, vascularity, proliferation rate, and survival of patients with invasive ductal carcinoma of the breast," *Cancer*, vol. 79, pp. 186–188, 1997.

[24] S. A. Feig *et al.*, "Thermography, mammography and clinical examination in breas screening," *Diag. Radiol*, vol. 122, pp. 123–127, 1977.

[25] C. J. Dowle, J. Caseldine, J. Tew, A. R. Manhire, E. J. Roebuck, and R. W. Blamey, "An evaluation of transmission spectroscopy (lightscanning) in the diagnosis of symptomatic breast lesions," *Clin. Radiol.*, vol. 38, pp. 375–377, 1987.

[26] R. J. Bartrum and J. C. Crow, "Transillumination lightscanning to diagnose breast cancer: A feasibility study," *Amer. J. Roentgen.*, vol. 142, pp. 409–414, 1984.

[27] E. A. Sickles, "Breast cancer detection with transillumination and mammography," *Amer. J. Roentgen.*, vol. 142, pp. 841–848, 1983.

[28] G. E. Geslien, J. R. Fisher, and C. Delaney, "Transillumination in breast cancer detection: Screening failures and potential," *Amer. J. Roentgen.*, vol. 144, pp. 619–622, 1985.

[29] W. T. Joines, Y. Zhang, C. Li, and R. L. Jirtle, "The measured electrical properties of normal and malignant human tissues from 50 to 90 MHz," *Med. Phys.*, vol. 21, pp. 547–50, 1994.
[30] S. S. Chaudhury, R. K. Mishra, A. Swarup, and J. M. Thomas, "Dielectric properties of normal and malignant human breast tissues at radiowave and microwave frequencies," *Ind. J. Biochem. Biophys.*, vol. 21, pp. 76–79, 1984.
[31] J. Nuutinen, T. Lahtinen, M. Turunen, E. Alanen, M. Tenhunen, T. Usenius, and R. Kolle, "A dielectric method for measuring early and late reactions in irradiated human skin," *Radiotherapy Oncol.*, vol. 47, pp. 249–254, 1998.
[32] S. Caorsi, G. L. Gragnani, and M. P. Pastorino, "Reconstruction of dielectric permittivity distributions in arbitrary 2D inhomogeneous biological bodies by a multiview microwave numerical method," *IEEE Trans. Med. Imag.*, vol. 12, pp. 232–239, June 1993.
[33] N. Jaochimowicz, C. Pinchot, and R. Hugonin, "Inverse scattering: An iterative numerical method for electromagnetic imaging," *IEEE Trans. Antennas Propagat.*, vol. 39, pp. 1742–1752, 1991.
[34] C. Pichot and A. Franchois, "Microwave imaging-complex permittivity reconstruction with a Levenberg–Marquardt method," *IEEE Trans. Antennas Propagat.*, vol. 45, pp. 203–215, Feb. 1997.
[35] P. D. Meaney, K. D. Paulsen, and T. P. Ryan, "Two-dimensional hybrid element image reconstruction for TM illumination," *IEEE Trans. Antennas Propagat.*, vol. 43, pp. 239–247, Mar. 1995.
[36] A. Franchois, A. Joisel, C. Pichot, and J. C. Bolomey, "Quantitative microwave imaging with a 2.45-GHz planar microwave camera," *IEEE Trans. Med. Imag.*, vol. 17, pp. 550–561, Aug. 1998.
[37] P. M. Meaney, K. D. Paulsen, and J. Chang, "Near-field microwave imaging of biologically-based materials using a monopole system," *IEEE Trans. Microwave Theory Tech.*, vol. 46, pp. 31–45, Jan. 1998.
[38] P. M. Meaney, K. D. Paulsen, J. T. Chang, M. W. Fanning, and A. Hartov, "Compensation for nonactive array element effects in a microwave imaging system: Part II—Imaging results," *IEEE Trans. Med. Imaging*, vol. 18, pp. 508–518, June 1999.
[39] P. M. Meaney, K. D. Paulson, A. Hartov, and R. K. Crane, "Multi-target microwave imaging for tissue assessment: Initial evaluation in tissue-equivalent phantoms," *IEEE Trans. Biomed. Eng.*, vol. 43, pp. 878–890, Sept. 1996.
[40] S. C. Hagness, A. Taflove, and J. E. Bridges, "Three-dimensional FDTD Analysis of a pulsed microwave confocal system for breast cancer detection: Design of an antenna-array element," *IEEE Trans. Antennas Propagat.*, vol. 47, pp. 783–791, May 1999.
[41] ——, "Two-dimensional FDTD analysis of a pulsed microwave confocal system for breast cancer detection: Fixed-focus and antenna-array sensors," *IEEE Trans. Biomed. Eng.*, vol. 45, pp. 1470–1479, Dec. 1998.
[42] E. C. Fear and M. A. Stuchly, "Microwave system for breast tumor detection," *IEEE Microwave Guided Lett.*, vol. 9, pp. 470–472, Nov. 1999.
[43] P. M. Meaney, K. D. Paulsen, A. Hartov, and R. C. Crane, "An active microwave imaging system for reconstruction of 2-D electrical property distributions," *IEEE Trans. Biomed. Imag.*, vol. 42, pp. 1017–1026, Oct. 1995.
[44] K. D. Paulsen and P. M. Meaney, "Compensation for nonactive array element effects in a microwave imaging system: Part I—Forward solution vs. measured data comparison," *IEEE Trans. Med. Imag.*, vol. 18, pp. 496–507, June 1999.
[45] D. R. White, H. Q. Woodard, and S. M. Hammond, "Average soft-tissue and bone models for use in radiation dosimetry," *Br. J. Radiol.*, vol. 60, pp. 903–913, 1987.
[46] H. Q. Woodard and D. R. White, "The composition of body tissues," *Br. J. Radiol.*, vol. 59, pp. 1209–1219, 1986.
[47] L. C. Junqueira, J. Carneiro, and R. Kelley, *Basic Histology*, 8th ed. Norwalk, CT: Appleton & Lange, 1995, pp. 443–446.
[48] C. Beckmann *et al.*, *Obstetrics & Gynecology*, 2nd ed. Baltimore, MD: Williams & Wilkins, 1992, pp. 235–238.
[49] A. Scharzberg and A. J. Devaney, "Super-resolution in diffraction tomography," *Inverse Problems*, vol. 8, pp. 149–164, 1992.
[50] W. C. Chew, Y. M. Wang, G. Otto, D. Lesselier, and J. C. Bolomey, "On the inverse source method of solving inverse scattering problems," *Inverse Problems*, vol. 10, pp. 547–553, 1994.
[51] M. Bertero, P. Boccacci, and M. Piana, "Resolution and super-resolution in inverse diffraction," in *Proc. Inverse Problems Wave Propagat. Diffraction*, Aix-les-Bains, France, 1996, pp. 1–17.
[52] W. C. Chew, G. P. Otto, W. H. Weedon, J. H. Lin, C. C. Lu, Y. M. Wang, and M. Moghaddam, "Nonlinear diffraction tomography: The use of inverse scattering for imaging," *Int. J. Imaging Syst. Technol.*, vol. 7, pp. 16–24, 1996.
[53] P. Lobel, C. Pichot, L. Blanc-Feraud, and M. Barlaud, "Conjugate-gradient algorithm with edge-preserving regularization for image reconstruction from Ipswich data for mystery objects," *IEEE Antennas Propagat. Mag.*, vol. 39, pp. 12–14, Jan. 1997.
[54] P. M. Meaney, K. D. Paulsen, M. W. Fanning, and J. T. Chang, "Advances in microwave imaging for clinical implementations in breast tumor detection and thermal therapy monitoring," *Recent Res. Development Microwave Theory Tech.*, vol. 1, pp. 37–56, 1999.

**Paul M. Meaney** (S'91–M'95), photograph and biography not available at time of publication.

**Margaret W. Fanning**, photograph and biography not available at time of publication.

**Dun Li**, photograph and biography not available at time of publication.

**Steven P. Poplack**, photograph and biography not available at time of publication.

**Keith D. Paulsen** (S'85–M'86), photograph and biography not available at time of publication.